Hindawi
Advances in Materials Science and Engineering
Volume 2022, Article ID 2779965, 16 pages
https://doi.org/10.1155/2022/2779965

Research Article

Development and Application of Analogous Materials for Fluid-Solid Coupling Physical Model Test

Mingyang Ren,[1] **Xiangjie Yin**,[2] **Ningjing Li**,[3] **Xuyang Wu**,[1] **and Heng Liu**[1]

[1]*School of Civil and Transportation Engineering, Henan University of Urban Construction, Pingdingshan, Henan, China*
[2]*Lixia Holding, Jinan, China*
[3]*China Petroleum Pipeline Engineering Corporation, Langfang, Hebei, China*

Correspondence should be addressed to Mingyang Ren; 20201017@hncj.edu.cn

Received 3 August 2022; Accepted 26 September 2022; Published 10 October 2022

Academic Editor: Depeng Ma

The coupling effect between the stress field formed by rock mass and the seepage field formed by groundwater has an important impact on the stability of underground engineering. In order to conduct the fluid-solid coupling physical model test in the laboratory, it is necessary to develop suitable analogous materials. In this study, a new type of analogous material reflecting the fluid-solid coupling effect is developed with iron powder, barite powder, and quartz sand as aggregates, white cement as a cementing agent, and silicone oil as a regulator. Through a large number of orthogonal experiments, the influence laws of different material contents on the mechanical properties and permeability characteristics of analogous materials are obtained. In addition, a method for quickly determining the proportion of components in fluid-solid coupling analogous materials is also proposed. The developed analogous material is employed in the fluid-solid coupling physical model test of a deep tunnel. The variation laws of rock stress, displacement, and seepage pressure around the tunnel during construction are obtained, which verifies the feasibility of the developed analogous material.

1. Introduction

With the rapid development of the global economy and the gradual expansion of human living space, many underground projects under construction and planning continue to march into the deep rock mass. In the fields of mining, transportation, water conservancy and hydropower, energy, and nuclear waste disposal, the buried depth of underground tunnels or caverns has reached more than 1000 kilometers. With the increase in buried depth, the stability of underground engineering is greatly threatened, especially the coupling effect of high ground stress and high external water pressure [1–5]. Therefore, it is of great significance for the safety and economy of underground engineering to study the distribution and evolution of stress, seepage pressure, and displacement in deep rock mass under fluid-solid coupling conditions.

For the complex coupling between the stress field and seepage field of rock mass, theoretical analysis, numerical simulation, and geomechanical model testing are the three main research methods. Moreover, the geomechanical model test can truly reflect the spatial relationship between geological structure and engineering structure and accurately simulate the construction process. Especially, for large and complex engineering problems, it plays an irreplaceable role than theoretical analysis and numerical simulation [6, 7]. The success of the fluid-solid coupling model test of deep rock mass mainly depends on the reliability of the fluid-solid coupling similarity criterion and fluid-solid coupling analogous materials. At present, scholars have studied the fluid-solid coupling similarity theory and analogous materials around these two aspects. Based on the fluid-solid coupling similarity criterion of continuum mechanics theory, Li et al. [8–10] developed a fluid-solid coupling analogous material composed of sand, barite powder, talc powder, cement, petrolatum, silicone oil, and an appropriate amount of mixing water, which can simulate different rock masses with different permeabilities. Hu et al. [11] systematically discussed the three-dimensional solid-fluid coupling similarity theory, which provided theoretical

guidance for the development of model test technology. From the perspective of fluid-solid coupling theory, Chen et al. [12] developed a kind of fluid-solid coupling analogous material for deep water barriers with paraffin and Vaseline as cementing agents, river sand and calcium carbonate as aggregates, and hydraulic oil as a regulator. Yu et al. [13] employed low-melting, high-quality paraffin as a binder, sand and talc powder as aggregate, and high-quality wear-resistant hydraulic oil as the regulator and developed a nonhydrophilic fluid-solid coupling analogous material. Bai et al. [14] developed a novel analogous material mixed with calcium carbonate, white cement, paraffin, quartz sand, silicone oil, talc, and iron powder and researched the effects of different mixing ratios on the mechanical properties of the analogous material. Based on the fluid-solid coupling similarity theory of continuous media, S. Liu and W. Liu [15] mixed river sand, calcium carbonate, talc powder, white cement, Vaseline, and hydraulic oil and developed a fluid-solid coupling analogous material that can simulate coal seam aquifers. Shi et al. [16] developed an analogous material with cement and gypsum as cementing agents and quartz sand as aggregate and studied the relationship between water absorption, softening coefficient, permeability coefficient, sand binder ratio, water paste ratio, and quartz sand particle size. Using cement and gypsum as cementing materials and sand as aggregate, Huang et al. [17] formulated a fluid-solid coupling analogous material that can simulate water inrush in tunnels under excavation disturbance.

Although some progress has been made in the study of fluid-solid coupling analogous materials, the current fluid-solid coupling analogous materials are based on the theory of continuum mechanics without considering the effects of high ground stress [18–24]. The existing fluid-solid coupling analogous materials are not suitable for high ground stress environments. Therefore, this study firstly deduces the fluid-solid coupling similarity criterion under high in situ stress and high water pressure. Then, under the guidance of the derived similarity criterion, a new type of fluid-solid coupled analogous material suitable for simulating deep rock mass engineering is developed, and the effects of different mixing ratios on the density, compressive strength, tensile strength, deformation modulus, and permeability coefficient of analogous materials are studied through orthogonal tests. Finally, taking Xianglu Mountain Tunnel as the engineering background, the effectiveness of the developed analogous material is verified by conducting a fluid-solid coupling model test.

2. Fluid-Solid Coupling Similarity Conditions under High In Situ Stress

According to the similarity principle, the fluid-solid coupling model test of deep rock mass must not only meet the similarity of geometric dimensions, boundary conditions, mechanical properties, and rock mass structure but also meet the similarity of hydraulic properties (mainly referring to the four parameters including permeability coefficient, seepage pressure, seepage flow, and flow velocity).

The fluid-solid coupling similarity criterion is the basis for the development of analogous materials. The current fluid-solid coupling similarity criterion is mostly derived from the homogeneous continuum mechanics model [11], which is expressed as follows:

$$\begin{cases} C_G \dfrac{C_\delta}{C_L^2} = C_\lambda \dfrac{C_V}{C_L} = C_G \dfrac{C_V}{C_L} = C_\rho \dfrac{C_\delta}{C_t^2} = C_\gamma \\ C_K = \sqrt{C_L}/C_\gamma \\ C_P = C_\gamma C_L \end{cases}, \tag{1}$$

where C_G is the similarity ratio of shear modulus, C_δ is the similarity ratio of displacement, C_L is the similarity ratio of geometric dimensions, C_λ is the similarity ratio of Lame's constant, C_V is the similarity ratio of volume, C_ρ is the similarity ratio of density, C_t is the similarity ratio of time, C_γ is the similarity ratio of unit weight, C_K is the similarity ratio of permeability coefficient, and C_P is the similarity ratio of seepage pressure.

When the rock mass is under the influence of high in situ stress and high seepage pressure, the similarity relationship of equation (1) will no longer be satisfied. Therefore, it is necessary to establish the fluid-solid coupling similarity criterion considering high in situ stress and high seepage pressure.

2.1. Similarity Criterion of Permeability Coefficient. Considering the influence of high ground stress on the permeability coefficient, Wu et al. [25] obtained the relationship between effective stress and permeability coefficient through a large number of field tests:

$$K_f = K_0 \sigma^{-a}, \tag{2}$$

where K_f is the permeability coefficient, K_0 is the permeability coefficient when the effective stress approaches 0, σ is the effective stress, and α is the fractal dimension of fracture distribution density.

In order to keep the dimension consistent, $\sigma_0 = 1$ MPa is introduced; then, equation (2) can be rewritten as

$$K_f = K_0 \left(\frac{\sigma}{\sigma_0}\right)^{-a}. \tag{3}$$

Combining equation (3) and similarity principle, we can obtain

$$\text{Prototype: } K_f = K_0 \left(\frac{\sigma}{\sigma_0}\right)^{-a} (\sigma > 0), \tag{4}$$

$$\text{Mo de l: } K_f' = K_0' \left(\frac{\sigma'}{\sigma_0'}\right)^{-a'} (\sigma' > 0). \tag{5}$$

According to the similarity principle and in combination with equations (4) and (5), it can be deduced that

$$C_{K_f}K_f' = C_{K_0}K_0'\left(\frac{C_\sigma\sigma'}{C_{\sigma_0}\sigma_0'}\right)^{-C_a a'}. \quad (6)$$

Since α is a dimensionless quantity and σ_0 is a constant, we get $C_\alpha = 1$ and $C_{\sigma 0} = 1$. Therefore, equation (6) can be simplified as

$$\frac{C_K}{C_{K_0}C_\sigma^{-\alpha}}K_f' = K_0'\sigma'^{-\alpha'}. \quad (7)$$

So, the similarity ratio of permeability coefficient considering the influence of high stress is

$$C_K = C_{K_0}C_\sigma^{-\alpha}. \quad (8)$$

The similarity ratio formula of permeability coefficient in equation (1) is brought into equation (8), and the similarity condition of permeability coefficient considering high in situ stress is

$$C_K = C_\sigma^{-\alpha}C_\gamma^{-1}C_L^{1/2}. \quad (9)$$

2.2. Similarity Criterion of Seepage Flow. The relationship between the similarity ratio of seepage flow and permeability coefficient is

$$\text{Prototype: } Q = K_f A\frac{H_1 - H_2}{L}, \quad (10)$$

$$\text{Model: } Q' = K_f'A'\frac{H_1' - H_2'}{L'}, \quad (11)$$

where Q is the seepage discharge, K_f is the permeability coefficient, H_1 and H_2 are the water head heights along the seepage path, respectively, L is the length of seepage path, and A is the seepage cross-sectional area. According to the similarity principle, we can obtain

$$C_Q Q' = C_{K_f}K_f'C_L^2A'\frac{C_L H_1' - C_L H_2'}{C_L L'}. \quad (12)$$

After simplifying equation (12), it can be deduced that

$$C_Q = C_K C_L^2. \quad (13)$$

Taking equation (9) into (13), the similarity condition of seepage flow considering the influence of high ground stress is

$$C_Q = C_\sigma^{-\alpha}C_\gamma^{-1}C_L^{2/5}. \quad (14)$$

2.3. Similarity Criterion of Flow Velocity. The calculation formula of fluid velocity is

$$v = \frac{L}{t}, \quad (15)$$

where v is the velocity of the fluid, L is the movement path of the fluid, and t is the movement time of the fluid.

According to the similarity theory, the similarity ratios of flow velocity and acceleration satisfy

$$C_v = \frac{C_L}{C_t}, \quad (16)$$

$$C_a = \frac{C_v}{C_t} = \frac{C_v^2}{C_L}. \quad (17)$$

The gravity of two similar flow fields in the gravity field must also be similar. Therefore, the following formula holds

$$C_a = \frac{C_v}{C_t} = \frac{C_v^2}{C_L} = C_g. \quad (18)$$

Therefore, the similarity ratio relation of flow velocity is

$$C_v = \sqrt{C_L C_g}. \quad (19)$$

2.4. Similarity Criterion of Seepage Pressure. According to the definition of seepage pressure and the similarity principle, the following formula can be deduced:

$$\text{Prototype: } P = \frac{F}{A}, \quad (20)$$

$$\text{Model: } P' = \frac{F'}{A'}. \quad (21)$$

$$\begin{cases} P = C_P P' \\ F = C_F F' \\ A = C_A A' \end{cases}. \quad (22)$$

Combined with equation (20)–(22), the following formulas can be deduced:

$$C_P = \frac{C_F}{C_A} = \frac{C_F}{C_L^2}. \quad (23)$$

The similarity ratio of forces can be deduced as

$$C_F = \frac{\rho L^{3v/t}}{\rho' L'^{3v'/t'}} = C_\gamma C_L^2 C_v^2. \quad (24)$$

Combined with equations (23) and (24), the relationship of similarity ratio between seepage pressure and flow velocity is

$$C_P = C_\gamma C_v^2. \quad (25)$$

So, similar condition of seepage pressure can be written as

$$C_P = C_\gamma C_L. \quad (26)$$

3. Development of Fluid-Solid Coupling Analogous Materials

3.1. Selection of Raw Materials. The raw materials of fluid-solid coupling analogous materials mainly include aggregate,

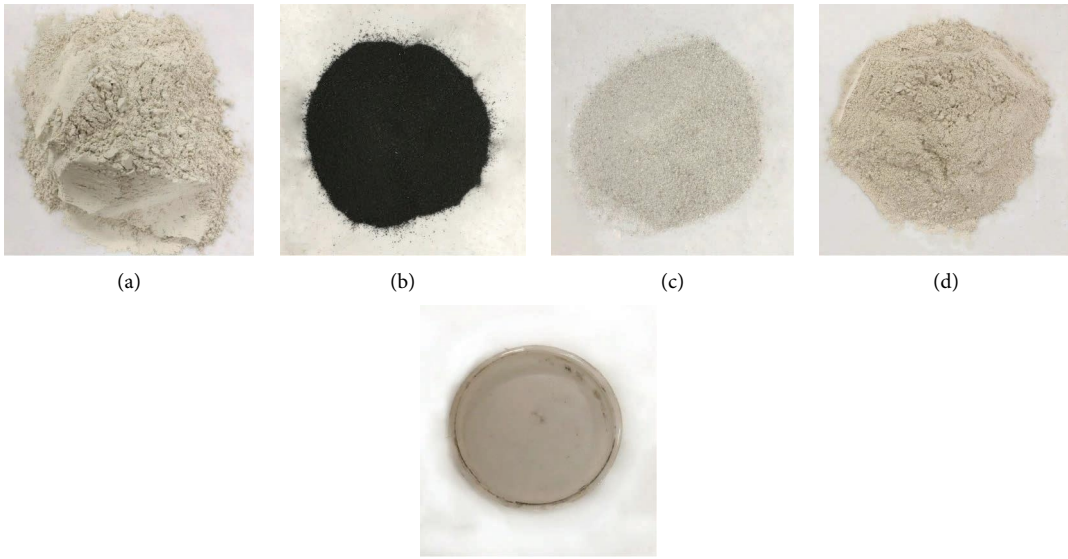

(a) (b) (c) (d)

(e)

Figure 1: Raw materials used for developing fluid-solid coupling analogous materials. (a) Barite powder; (b) iron powder; (c) quartz sand; (d) white cement; (e) silicone oil.

cementing agent, and regulator. By consulting a large number of literature on fluid-solid coupling analogous materials and testing the relevant characteristics of raw materials [7–10], it is finally determined to select iron powder, quartz sand and barite powder as aggregates, white cement as a cementing agent, and silicone oil as a regulator to develop fluid-solid coupling analogous materials.

As the main raw material, aggregate plays the role of skeleton and support for the specimen. If no aggregate is added during the production of the test sample, the test sample will not be formed. In our test, the grain size of quartz sand particles is in the range of 300~1200 μm, the grain size of barite powder is in the range of 20~70 μm, and iron powder has a particle size in the range of 80~130 μm. A cementing agent refers to a substance with considerable strength that changes the properties of the material through physical and chemical actions and can be closely bonded with other materials. The cementation strength of white cement is between gypsum and cement, which can better adjust the strength of analogous materials. So, the materials will not collapse in the case of water and meet the two special conditions of deformation and permeability. In the development of fluid-solid coupling analogous materials, the role of the regulator is generally to adjust the permeability coefficient of materials. In this study, high-quality silicone oil with a viscosity of 10^{-3} m^2/s is selected, which has the functions of moisturizing and reducing dry cracking, and can improve the nonhydrophilic property of the material. Figure 1 illustrates the raw materials used for developing fluid-solid coupling analogous materials.

3.2. Experimental Scheme and Sample Preparation for Analogous Materials. The influence of components in raw materials on the mechanical properties and hydraulic properties of fluid-solid coupling analogous materials is studied by an orthogonal test. In the orthogonal experiment, the mass ratio of iron powder, quartz sand, and barite powder is selected as factor A, the ratio of white cement mass to aggregate mass is selected as factor B, and the ratio of silicone oil mass to aggregate mass is selected as factor C. Due to the important influence of aggregate on materials, factor A is set at 7 levels: 1 : 1 : 1, 2 : 1 : 1, 4 : 1 : 1, 1 : 2 : 1, 1 : 4 : 1, 1 : 1 : 2, and 1 : 1 : 4. Factor B is set at 4 levels of 0.1%, 2%, 4%, and 6%. Factor C is set at 4 levels of 0.1%, 3%, 6%, and 9%. The designed orthogonal experimental scheme L_{32} ($1^7 \times 2^4$) is listed in Table 1.

Fluid-solid coupling analogous material tests include density test, uniaxial compression test, Brazilian splitting test, and permeability test, which are used to obtain its density, compressive strength, tensile strength, deformation modulus, and permeability coefficient. Figure 2 displays the preparation of fluid-solid coupling analogous material specimens. Figure 3 gives the process of testing analogous materials.

Figure 4 presents the axial stress-axial strain curve from uniaxial compression test. It can be seen that the axial stress-axial strain curve of analogous materials shows obvious strain softening characteristics, which is similar to the complete stress-strain curve of rock.

According to the orthogonal experimental scheme designed in Table 1, the density, uniaxial compressive strength, tensile strength, deformation modulus, and permeability coefficient of each group of fluid-solid coupling analogous materials are listed in Table 2.

4. Influence of Components in Raw Materials on Properties of Analogous Materials

Range is the reflection of the influence of different levels on specific test indicators under specific factors. For the results

Table 1: Orthogonal experimental scheme L_{32} ($1^7 \times 2^4$).

Experiment number	Experimental scheme	Mass ratio Iron powder : quartz sand : barite powder	Ratio of white cement mass to aggregate mass (%)	Ratio of silicone oil mass to aggregate mass (%)
1	A_1—B_1—C_1	1 : 1 : 1	0.1	0.1
2	A_1—B_1—C_4	1 : 1 : 1	0.1	9
3	A_1—B_2—C_2	1 : 1 : 1	2	3
4	A_1—B_2—C_3	1 : 1 : 1	2	6
5	A_1—B_3—C_2	1 : 1 : 1	4	3
6	A_1—B_3—C_3	1 : 1 : 1	4	6
7	A_1—B_4—C_4	1 : 1 : 1	6	9
8	A_1—B_4—C_1	1 : 1 : 1	6	0.1
9	A_2—B_1—C_3	2 : 1 : 1	0.1	6
10	A_2—B_2—C_4	2 : 1 : 1	2	9
11	A_2—B_3—C_1	2 : 1 : 1	4	0.1
12	A_2—B_4—C_2	2 : 1 : 1	6	3
13	A_3—B_1—C_1	4 : 1 : 1	0.1	0.1
14	A_3—B_2—C_2	4 : 1 : 1	2	3
15	A_3—B_3—C_3	4 : 1 : 1	4	6
16	A_3—B_4—C_4	4 : 1 : 1	6	9
17	A_4—B_1—C_3	1 : 2 : 1	0.1	6
18	A_4—B_2—C_4	1 : 2 : 1	2	9
19	A_4—B_3—C_1	1 : 2 : 1	4	0.1
20	A_4—B_4—C_2	1 : 2 : 1	6	3
21	A_5—B_1—C_2	1 : 4 : 1	0.1	3
22	A_5—B_2—C_1	1 : 4 : 1	2	0.1
23	A_5—B_3—C_4	1 : 4 : 1	4	9
24	A_5—B_4—C_3	1 : 4 : 1	6	6
25	A_6—B_1—C_4	1 : 1 : 2	0.1	9
26	A_6—B_2—C_3	1 : 1 : 2	2	6
27	A_6—B_3—C_2	1 : 1 : 2	4	3
28	A_6—B_4—C_1	1 : 1 : 2	6	0.1
29	A_7—B_1—C_2	1 : 1 : 4	0.1	3
30	A_7—B_2—C_1	1 : 1 : 4	2	0.1
31	A_7—B_3—C_4	1 : 1 : 4	4	9
32	A_7—B_4—C_3	1 : 1 : 4	6	6

(a) (b) (c)

Figure 2: Preparation of fluid-solid coupling analogous material specimens. (a) Dumping mixed materials; (b) compression moulding; (c) cured specimen.

of orthogonal test, the range analysis method is intuitive and easy to understand. The primary and secondary factors affecting the test results can be easily obtained through range analysis.

When the levels of each factor in the orthogonal experimental scheme are equal, the sensitivity order of all factors is completely determined by the range. Since the level of factor A in our orthogonal experiment is 7, the level of other factors is 4. Therefore, the range of factor A needs to be reduced. The reduction formula of the range is

$$R' = dR\sqrt{r}, \tag{27}$$

Figure 3: Process of testing analogous materials. (a) Uniaxial compression test; (b) failed specimen after compression; (c) brazilian splitting test; (d) permeability test.

where R' and R are the range before and after reduction, respectively, r is the repetition times of each level test of this factor, $r = n/m$, n is the number of tests, m is the number of levels, and d is the reduced coefficient, which is related to the level number of factor.

4.1. Influence of Material Components on Density. Table 3 and Figure 5 display the influence of material composition on density. From Table 3, it can be seen that the density is most affected by aggregate, followed by silicone oil, and least by white cement. Moreover, compared with silicone oil and white cement, aggregate has a dominant effect on density. The effect of white cement on density is almost negligible. The variation curves of density with various factors in Figure 5 can also prove this point. In addition, with the increase in the proportion of iron powder, the density of analogous materials showed a significant increasing trend. This is mainly due to the fact that the density of the iron powder is much higher than that of other components. Therefore, this can give us an enlightenment; when matching fluid-solid coupling analogous materials, the density of the analogous material can be adjusted by controlling the content of the iron powder.

4.2. Influence of Material Components on Compressive Strength. Table 4 and Figure 6 display the influence of material composition on compressive strength. From Table 4, it can be seen that the ranges of three factors *A*, *B,* and *C* are 0.33 MPa, 0.85 MPa, and 0.06 MPa, respectively. Therefore, the compressive strength is most affected by white cement, followed by aggregate, and least by silicone oil. Moreover, the effect of white cement on compressive

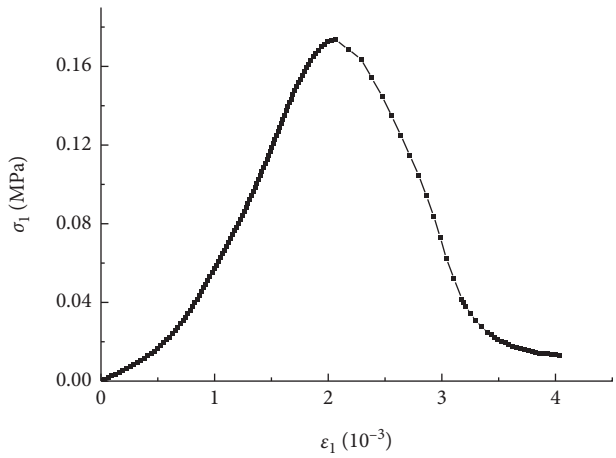

Figure 4: Axial stress-axial strain curve of fluid-solid coupling analogous material.

Table 2: Orthogonal experimental result.

Experiment number	Density (g/cm^3)	Compressive strength (MPa)	Tensile strength (kPa)	Deformation modulus (MPa)	Permeability coefficient (m/s)
1	2.51	0.51	71.3	86.5	$9.60e^{-8}$
2	2.7	0.65	30.2	101.4	$5.20e^{-8}$
3	2.61	0.91	50.6	77.3	$6.80e^{-8}$
4	2.65	0.98	42.3	53.8	$5.30e^{-8}$
5	2.63	1.12	82.5	137.2	$3.90e^{-8}$
6	2.66	1.19	80.8	98.7	$2.10e^{-8}$
7	2.69	1.42	61.4	110.3	$9.10e^{-9}$
8	2.53	1.37	124.7	152.1	$6.80e^{-8}$
9	2.86	0.72	39.6	49.8	$4.13e^{-8}$
10	2.88	0.95	47.7	55.9	$7.10e^{-9}$
11	2.77	1.21	79.8	130.5	$8.90e^{-8}$
12	2.8	1.44	114.5	174.9	$9.30e^{-9}$
13	2.86	0.55	51.7	82.3	$8.30e^{-8}$
14	2.88	0.82	60.3	117.6	$3.30e^{-8}$
15	2.91	1.07	67.6	137.8	$1.10e^{-8}$
16	2.93	1.48	75.4	172.3	$9.50e^{-9}$
17	2.54	0.35	34.1	42.5	$3.50e^{-8}$
18	2.57	0.69	39.7	48.6	$1.10e^{-8}$
19	2.49	0.97	45.3	54.3	$7.10e^{-7}$
20	2.52	1.34	79.8	57.2	$2.00e^{-7}$
21	2.31	0.21	19.3	34.2	$9.20e^{-7}$
22	2.29	0.46	36.4	38.5	$9.60e^{-7}$
23	2.36	0.83	43.7	41.8	$1.40e^{-7}$
24	2.33	1.08	84.6	47.6	$1.10e^{-7}$
25	2.47	0.29	20.7	30.3	$3.20e^{-8}$
26	2.45	0.51	31.8	36.1	$1.20e^{-8}$
27	2.44	0.85	43.7	41.8	$2.85e^{-9}$
28	2.42	1.13	82.4	48.2	$5.20e^{-8}$
29	2.3	0.34	21.5	33.2	$1.70e^{-8}$
30	2.28	0.59	42.5	34.8	$5.80e^{-8}$
31	2.34	0.92	48.7	40.6	$1.00e^{-9}$
32	2.32	1.15	82.6	49.3	$8.90e^{-9}$

strength is much greater than that of aggregate and silicone oil. This can also be confirmed from the variation curves of compressive strength with various factors in Figure 6. Figure 6 clearly shows that the compressive strength first increases and then decreases with the increase of iron powder content. That is to say, there is a critical proportion (50%) of iron powder content in terms of compressive strength. In general, the compressive strength of analogous materials increases linearly with the increase of white cement content, but is not sensitive to the content of silicone oil.

Table 3: Range analysis of the influence of material composition on density.

Level number	Density (g/cm^3)		
	Factor *A*	Factor *B*	Factor *C*
1	2.62	2.57	2.52
2	2.83	2.58	2.56
3	2.90	2.58	2.59
4	2.53	2.57	2.62
5	2.32		
6	2.45		
7	2.31		
R	0.59	0.009	0.099
R′	0.44		

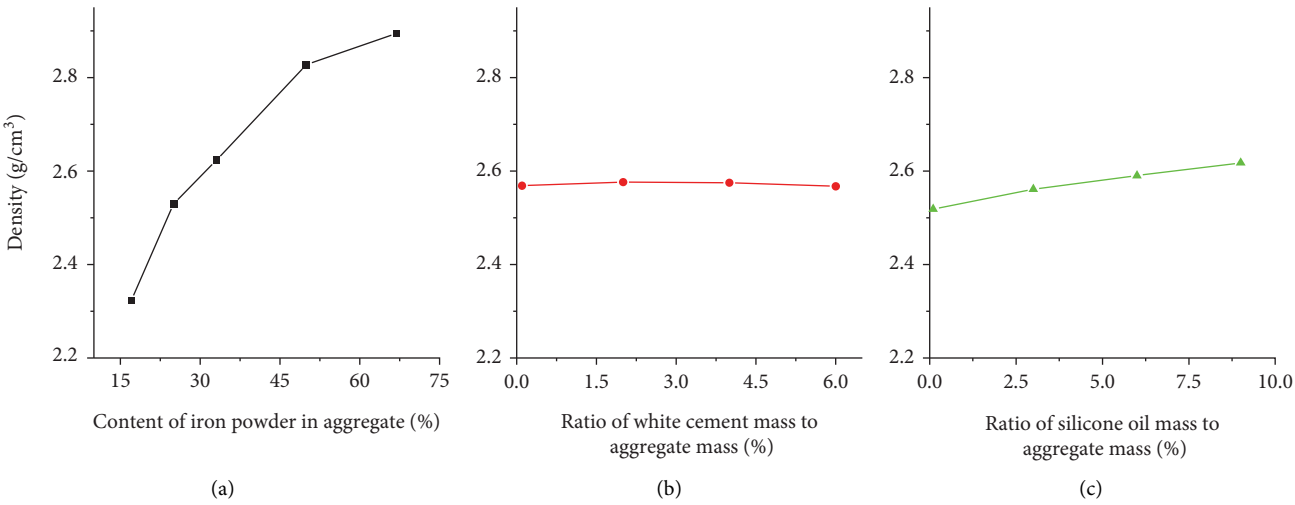

Figure 5: Influence of material composition on density.

Table 4: Range analysis of the influence of material composition on compressive strength.

Level number	Uniaxial compressive strength (MPa)		
	Factor *A*	Factor *B*	Factor *C*
1	1.02	0.45	0.85
2	1.08	0.74	0.88
3	0.98	1.02	0.88
4	0.84	1.30	0.90
5	0.65		
6	0.70		
7	0.75		
R	0.44	0.85	0.06
R′	0.33		

4.3. Influence of Material Components on Tensile Strength. Table 5 and Figure 7 display the influence of material composition on tensile strength. From Table 5, it can be seen that the ranges of three factors *A*, *B*, and *C* are 19.27 kPa, 52.13 kPa, and 20.83 kPa, respectively. Therefore, the tensile strength is most affected by white cement, which is consistent with its effect of compressive strength. In addition, the variation of tensile strength with the content of white cement and iron powder in Figure 7 is also consistent with the variation of compressive strength. However, the tensile strength decreases with the increase of silicone oil content. On the whole, both compressive strength and tensile strength are most affected by white cement. This also reflects the function of white cement as a cementing agent. Therefore, the strength of analogous materials can be adjusted by controlling the content of white cement.

4.4. Influence of Material Components on Deformation Modulus. Table 6 and Figure 8 display the influence of material composition on deformation modulus. From Table 6, it can be seen that the ranges of three factors *A*, *B*, and *C*

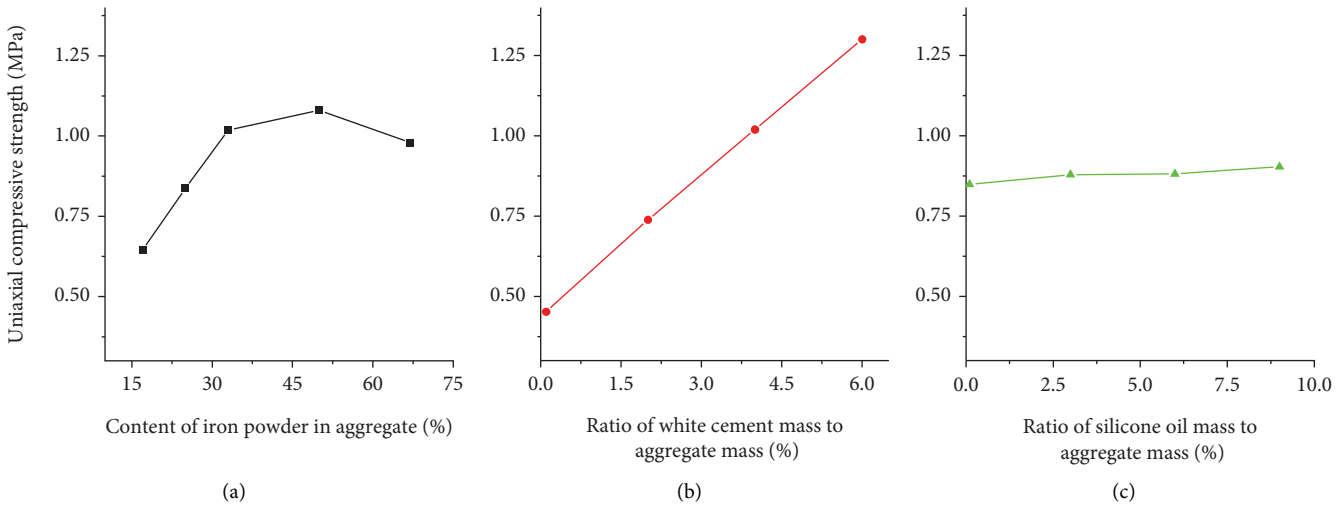

Figure 6: Influence of material composition on compressive strength.

Table 5: Range analysis of the influence of material composition on tensile strength.

Level number	Tensile strength (kPa)		
	Factor *A*	Factor *B*	Factor *C*
1	67.98	36.05	66.76
2	70.40	43.91	59.03
3	63.75	61.51	57.93
4	49.73	88.18	45.94
5	46.00		
6	44.65		
7	48.83		
R	25.75	52.13	20.83
R′	19.27		

are 66.15 MPa, 43.96 MPa, and 19.73 MPa, respectively. The influence of aggregate, white cement, and silicone oil on the deformation modulus decreases in turn. Figure 8 depicts that the deformation modulus generally increases with the increase of iron powder content and white cement content, but its change trend with silicone oil is not significant. The reason why the deformation modulus increases with the increase of iron powder content may be that iron powder improves the particle gradation of aggregate and increases its compactness. As a binder, white cement plays the role of bonding particles to stabilize the skeleton. The increase of its content will inevitably lead to the increase of deformation modulus.

4.5. Influence of Material Components on Permeability Coefficient. Table 7 and Figure 9 display the influence of material composition on permeability coefficient. From Table 6, it can be seen that the range of three factors *A*, *B*, and *C* are $3.83e^{-7}$ m/s, $1.01e^{-7}$ m/s, and $2.32e^{-7}$ m/s, respectively. Therefore, aggregate has the greatest influence on the permeability coefficient, followed by silicone oil, and white cement has the least influence. Figure 9 clearly shows that, with the increase of iron powder content, white cement content, and silicone oil content, the permeability coefficient of analogous materials shows a downward trend. The reason for this phenomenon may be that the increase in the content of iron powder improves the gradation of the particles of analogous materials and increases its compactness, while the increase in the content of white cement and silicone oil leads to the blockage of the permeable channels in the analogous materials, resulting in a decrease in the permeability coefficient. Different from the effect of white cement on the permeability coefficient, the effect of aggregate and silicone oil on the permeability coefficient has significant segmentation characteristics. For factor *A*, when the content of iron powder is lower than 33%, the change of permeability coefficient is very sharp, and when it exceeds 33%, the change of permeability coefficient is relatively gentle. Similarly, when the content of silicone oil is less than 6%, the permeability coefficient changes significantly, and when it is greater than 6%, the permeability coefficient basically remains unchanged. Therefore, the segmentation feature should be fully utilized when adjusting the permeability coefficient of fluid-solid coupling analogous materials.

To develop fluid-solid coupling analogous materials that meet certain requirements, it is usually necessary to carry out a large number of trial and error tests and repeatedly adjust the proportion of each material component. This is a rather

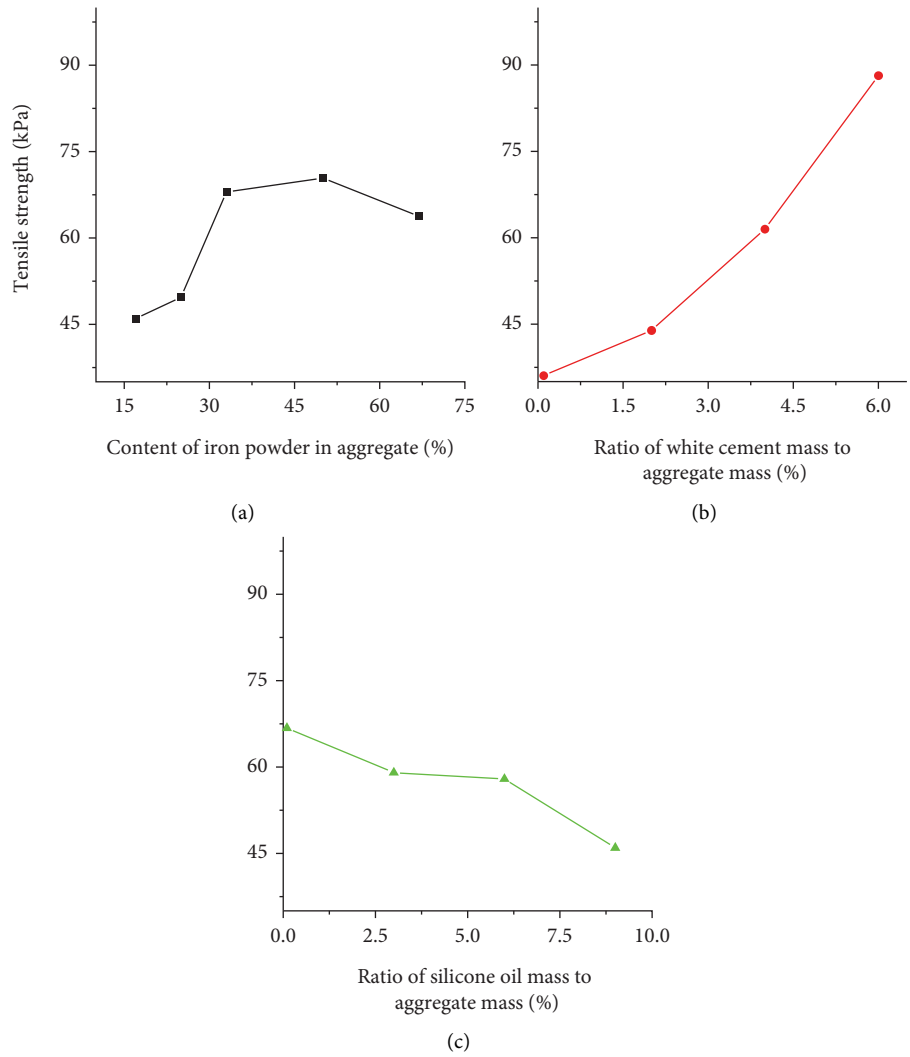

Figure 7: Influence of material composition on tensile strength.

Table 6: Range analysis of the influence of material composition on deformation modulus.

Level number	Deformation modulus (MPa)		
	Factor *A*	Factor *B*	Factor *C*
1	102.16	57.53	78.40
2	102.78	57.83	84.18
3	127.50	85.34	64.45
4	50.65	101.49	75.15
5	40.53		
6	39.10		
7	39.48		
R	88.40	43.96	19.73
R′	66.15		

tedious and arduous task. Therefore, based on the analysis of the influence of material components on the physical and mechanical properties of fluid-solid coupling analogous materials, we propose a method to quickly determine the proportion of components in analogous materials that meet certain requirements.

According to the above results, the role of aggregate is very important, especially the content of iron powder, which mainly affects the density, deformation modulus, and permeability of analogous materials. Therefore, the proportion of all components in aggregate is the main controlling factor in determining the proportioning

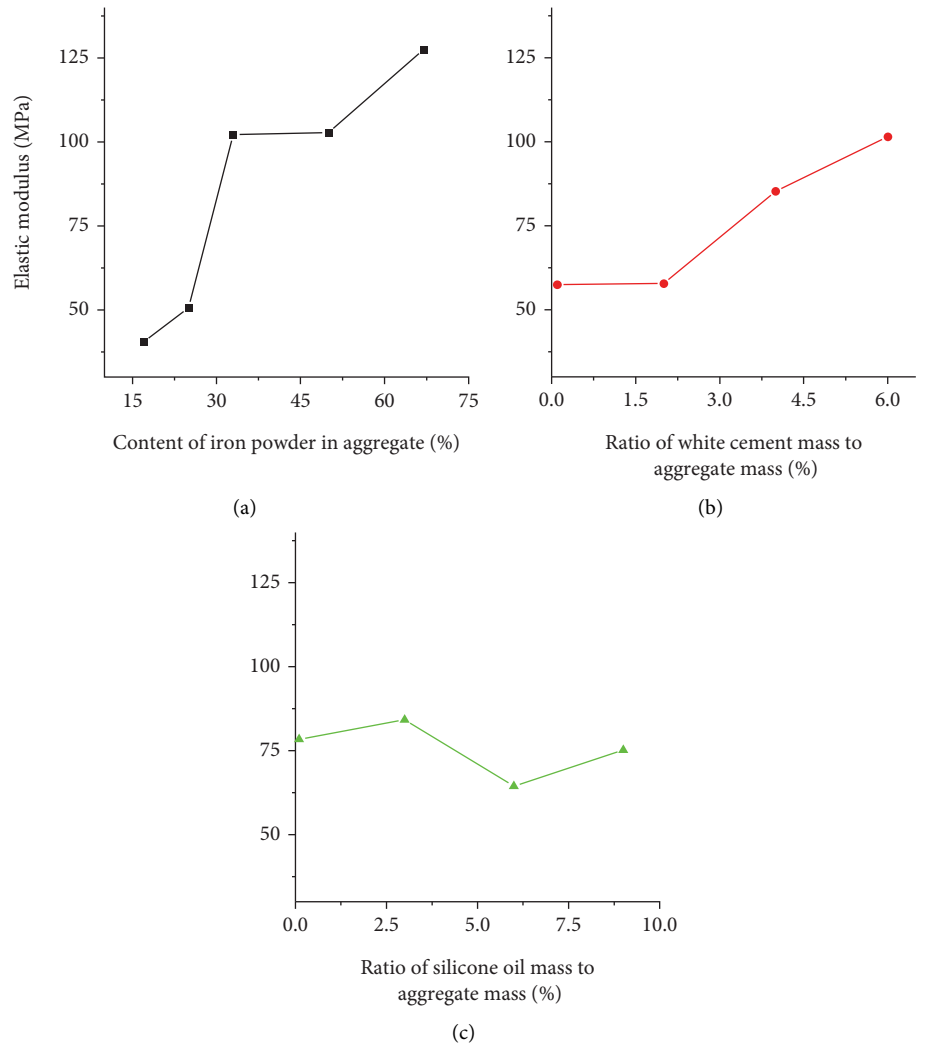

Figure 8: Influence of material composition on deformation modulus.

Table 7: Range analysis of the influence of material composition on permeability coefficient.

Level number	Permeability coefficient (m/s)		
	Factor A	Factor B	Factor C
1	$5.08e^{-8}$	$1.6e^{-7}$	$2.65e^{-7}$
2	$3.67e^{-8}$	$1.5e^{-7}$	$1.61e^{-7}$
3	$3.41e^{-8}$	$1.27e^{-7}$	$3.65e^{-8}$
4	$2.39e^{-7}$	$5.84e^{-8}$	$3.27e^{-8}$
5	$5.33e^{-7}$		
6	$2.47e^{-8}$		
7	$2.12e^{-8}$		
R	$5.11e^{-7}$	$1.01e^{-7}$	$2.32e^{-7}$
R'	$3.83e^{-7}$		

scheme of analogous material. White cement basically only controls the strength of the analogous material, while silicone oil mainly controls the permeability. Therefore, when formulating analogous materials, the approximate ratio range of each component in the aggregate should first be determined according to the desired density and deformation modulus. Secondly, the content range of white cement is determined according to the required compressive strength and tensile strength. Then, based on the desired permeability coefficient, the range of silicone oil content is roughly estimated. Finally, by fine-tuning the range of aggregate proportion, white cement content, and

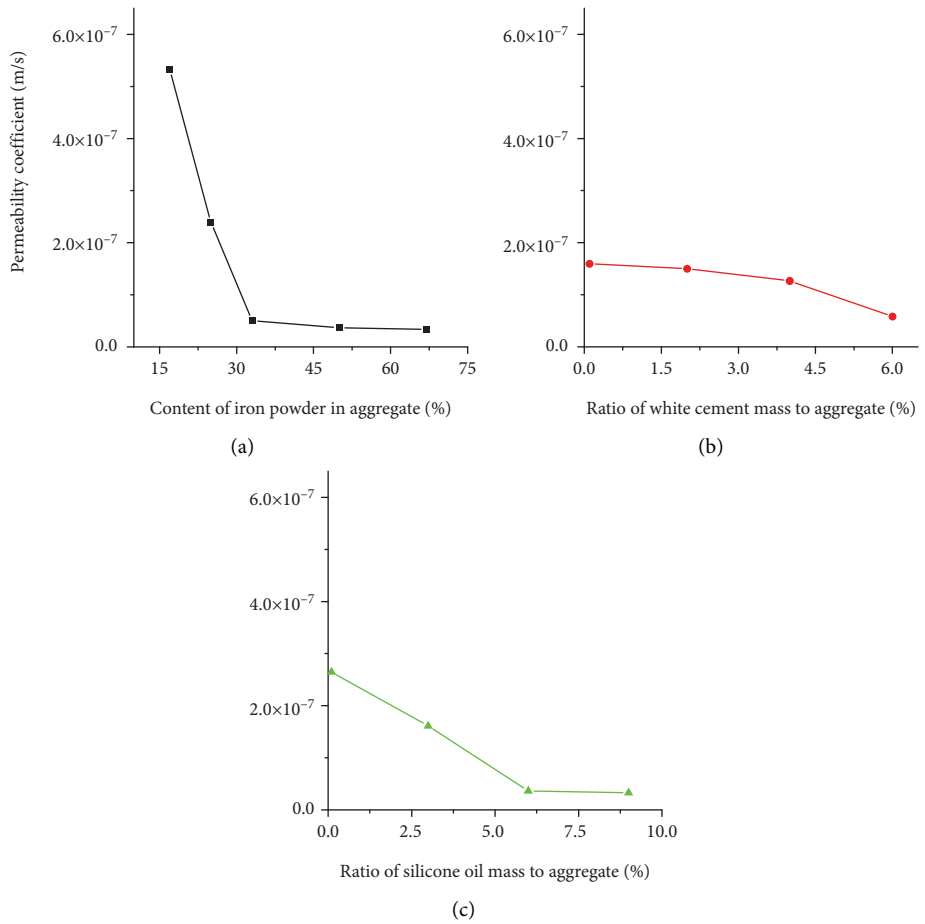

Figure 9: Influence of material composition on permeability coefficient.

silicone oil content, the proportion of each component of the fluid-solid coupling analogous material that meets the requirements can be quickly determined.

5. Application of Fluid-Solid Coupling Analogous Material

5.1. Model Test Overview. Taking Xianglu Mountain Tunnel as the engineering background, the fluid-solid coupling model test is carried out to verify the reliability of the developed fluid-solid coupling analogous material. Xianglu Mountain Tunnel is located in the first section of a large water diversion project in Yunnan Province, China. The tunnel has a total length of nearly 64 km and a maximum buried depth of nearly 1500 meters. It crosses the watershed of the Jinsha River and Lancang River. The geological conditions are very complex. There are many active faults along the tunnel line, and karst is relatively developed. When the tunnel crosses the fault fracture zone, major engineering geological disasters such as water and mud inrush may occur, which play a controlling role in the whole water diversion project [26, 27].

In this study, the typical deep-buried tunnel section (DL36 + 450-DL36 + 550) is selected to carry out the fluid-solid coupling model test. The buried depth of the tunnel in the test area is 1000~1250 m, and it crosses a fault with an inclination of 45° and a width of 15 m. The self-developed fluid-solid coupling true three-dimensional model test system was used in the test. According to the internal dimensions of the model box (length 1.0 m, width 1.0 m, and height 1.0 m) and the excavation requirements, the geometric similarity ratio is 100, the unit weight similarity ratio is 1, the stress similarity ratio is 100, and the permeability coefficient similarity ratio is 10.

According to the geological data, the physical and mechanical parameters of rocks inside and outside the fault are given in Table 8. Table 9 lists the proportion of components in analogous materials simulating rocks inside and outside the fault.

5.2. Model Test Process. The whole process of model testing is divided into the making of geological model, the installation of test elements, and the excavation and support of model tunnels. The geological model is made by layered compaction and layered air-drying curing. Since the test area contains a fault with an inclination of 45°, the test device shall be rotated by 45° before making the physical model (see Figure 10(a)). Then, the evenly mixed analogous material is paved in the model box (see Figure 10(b)). When the physical model is constructed to a specific height, the pressure cell, multipoint displacement meter, and seepage

Table 8: Physical and mechanical parameters of rocks inside and outside the fault.

Rock type	Density (g/cm^3)	Uniaxial compressive strength (MPa)	Tensile strength (kPa)	Deformation modulus (GPa)	Permeability coefficient (m/s)
Rock inside fault	2.6	44.7	2.8	11.6	$7.5e^{-7}$
Rock outside fault	2.5	18.2	1.2	3.9	$4.6e^{-6}$

Table 9: Proportion of components in analogous materials.

Material type	Mass ratio Iron powder : quartz sand : barite powder	Ratio of white cement mass to aggregate mass (%)	Ratio of silicone oil mass to aggregate mass (%)
Material inside fault	1.2 : 0.8 : 1.0	0.8	5.5
Material outside fault	0.4 : 0.6 : 1.0	0.5	3.1

(a)

(b)

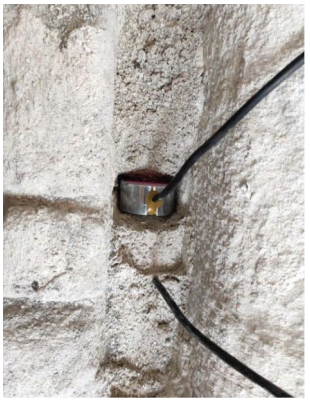

(c)

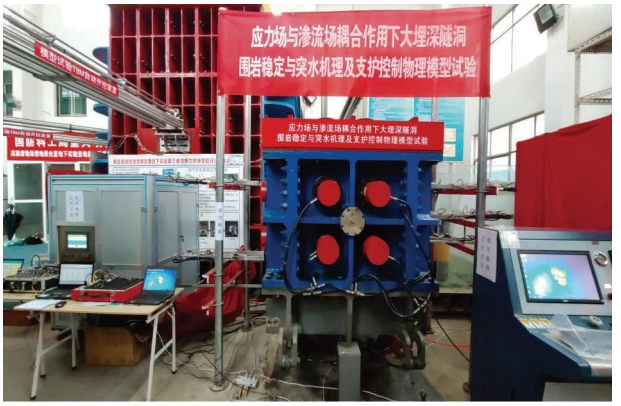

(d)

Figure 10: Continued.

(e) (f)

Figure 10: The process of fluid-solid coupling physical model test.

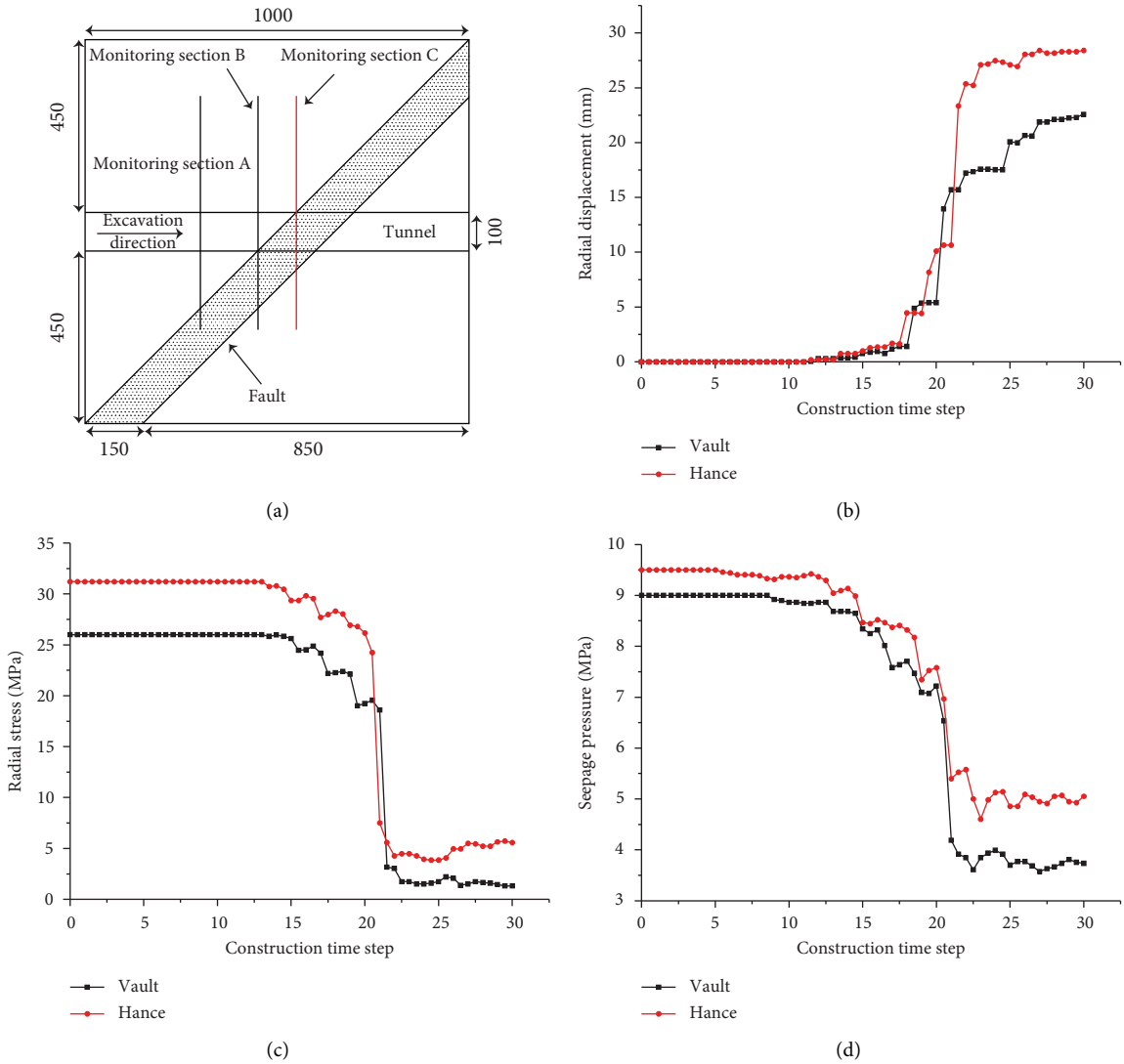

Figure 11: Variation curves of displacement, stress, and seepage pressure around the tunnel with construction time steps. (a) Monitoring section layout; (b) radial displacement; (c) radial stress; (d) seepage pressure.

pressure cell shall be buried around the tunnel (see Figure 10(c)). After the whole physical model is built, the boundary stress and water pressure need to be applied to the model to form a real stress environment and water environment in the physical model (see Figure 10(d)). Subsequently, special tools are used to excavate and support the model tunnel (see Figure 10(e)). Figure 10(f) shows the tunnel face after excavation. It can be clearly seen that there is seepage flow at the face, indicating that the developed analogous material can better simulate the seepage of groundwater.

5.3. Model Test Result. Taking monitoring Section 3 as an example, the variation curve of displacement, stress, and seepage pressure around the tunnel with the construction time step is shown in Figure 11. It can be clearly found that, with the advance of excavation, the radial deformation of rock around the tunnel increases gradually, while the radial stress and seepage pressure around the tunnel decreases gradually. After the support structure is installed, the deformation, stress, and seepage pressure of the surrounding rock gradually tend to be stable. These phenomena are consistent with common sense, which proves that the developed fluid-solid coupling analogous materials are feasible.

6. Conclusions

In this study, the fluid-solid coupling similarity conditions considering high in situ stress are derived. A new type of fluid-solid coupling analogous material is developed with iron powder, quartz sand, and barite powder as aggregates, white cement as a cementing agent, and silicone oil as a regulator and is applied to the fluid-solid coupling physical model test. The main conclusions are as follows:

(1) As three elements of analogous materials, the aggregate mainly affects the density and deformation characteristics, the white cement is mainly used to control the strength characteristics, and the role of the silicone oil is to adjust the permeability. Moreover, when the content of silicone oil is less than 6%, the permeability coefficient changes significantly. When its content is greater than 6%, the permeability coefficient basically remains unchanged.

(2) In order to quickly determine the proportion of all components in analogous materials that meet the requirements, the mass ratio of components in the aggregate should be determined first, followed by the content of white cement and finally the content of silicone oil.

(3) By using the developed materials to carry out physical model tests, the displacement, stress, and seepage pressure of rocks around the tunnel are accurately obtained. It proves the effectiveness of the developed materials.

Data Availability

The data presented in this study can be obtained from the corresponding author upon request.

Conflicts of Interest

The authors declare no conflicts of interest.

Acknowledgments

This research was funded by the https://doi.org/10.13039/501100001809Education Department of Henan Province of China (Grant no. 22A56008).

References

[1] H. Xie, T. Gao, and Y. Ju, "Research and development of rock mechanics in deep ground engineering," *Chinese Journal of Rock Mechanics and Engineering*, vol. 34, pp. 2161–2178, 2015.

[2] M. Wang, Z. Zhou, and Q. Qian, "Tectonic, deformation and failure problems of deep rock mass," *Chinese Journal of Rock Mechanics and Engineering*, vol. 23, pp. 448–455, 2006.

[3] L. Yuan, "Research progress of mining response and disaster prevention and control in deep coal mines," *Journal of China Coal Society*, vol. 46, pp. 716–725, 2021.

[4] M. He, "Progress and challenges of soft rock engineering in depth," *Journal of China Coal Society*, vol. 39, pp. 1409–1417, 2014.

[5] R. Yang, J. Lv, B. Zhou, and D. Ma, "Rock Unloading failure precursor based on Acoustic Emission Parametric fractal characteristics," *Lithosphere*, vol. 2022, Article ID 8221614, 2022.

[6] Y. Zhou, S. Li, L. Li, Q. Zhang, and S. Shi, "New technology for fluid-solid coupling tests of underground engineering and its application in experimental simulation of water inrush in filled-type karst conduit," *Chinese Journal of Geotechnical Engineering*, vol. 37, pp. 1232–1240, 2015.

[7] L. Li, S. Sun, J. Wang, W. Yang, S. Song, and Z. Fang, "Experimental study of the precursor information of the water inrush in shield tunnels due to the proximity of a water-filled cave," *International Journal of Rock Mechanics and Mining Sciences*, vol. 130, Article ID 104320, 2020.

[8] S. C. Li, H. L. Liu, L. P. Li, Q. Zhang, K. Wang, and K. Wang, "Large scale three dimensional seepage analysis model test and numerical simulation research on undersea tunnel," *Applied Ocean Research*, vol. 59, pp. 510–520, 2016.

[9] S. Li, D. Pan, and Z. Xu, "A model test on catastrophic evolution process of water inrush of a concealed Karst cave filled with confined water," *Rock and Soil Mechanics*, vol. 39, pp. 3164–3173, 2018.

[10] S. Li, C. Gao, Z. Zhou et al., "Analysis on the precursor information of water inrush in Karst tunnels: a true triaxial model test study," *Rock Mechanics and Rock Engineering*, vol. 52, no. 2, pp. 373–384, 2019.

[11] Y. Hu, Y. Zhao, and D. Yang, "Simulation theory and method of 3D solid-liquid coupling," *Journal of Liaoning Technical University*, vol. 26, pp. 204–206, 2007.

[12] J. Chen, L. Yin, and W. Sun, "Development and application for new solid-fluid coupling similar material of deep floor aquifuge," *Chinese Journal of Rock Mechanics and Engineering*, vol. 34, pp. 3956–3964, 2015.

[13] L. Yu, H. Jing, and B. Xu, "Solid-fluid coupling analogous material test for subsea tunnel," *Journal of Central South University*, vol. 46, pp. 983–990, 2015.

[14] J. Bai, M. Wang, Q. S. Zhang, Z. Zhu, R. Liu, and W. Li, "Development and application of a new similar material for fluid–solid coupling model test," *Arabian Journal of Geosciences*, vol. 13, no. 18, p. 913, 2020.

[15] S. Liu and W. Liu, "Experimental development process of a new fluid-solid coupling similar-material based on the orthogonal test," *Processes*, vol. 6, no. 11, p. 211, 2018.
[16] X. Shi, B. Liu, and Y. Qi, "Applicability of similar materials bonded by cement and plaster in solid-liquid coupling tests," *Rock and Soil Mechanics*, vol. 36, pp. 2624–2630, 2015.
[17] Z. Huang, X. Li, and S. Li, "Research and development of similar material for liquid-solid coupling and its application in tunnel water-inrush model test," *Journal of Central South University*, vol. 49, pp. 3029–3039, 2018.
[18] S. Li, X. Feng, S. Li, L. Li, and G. Li, "Research and development of a new similar material for solid-fluid coupling and its application," *Chinese Journal of Rock Mechanics and Engineering*, vol. 29, pp. 281–288, 2010.
[19] Z. Liu and Y. Hu, "Solid liquid coupling study on water inrush through faults in coal mining above confined aquifer," *Journal of China Coal Society*, vol. 32, pp. 1046–1050, 2007.
[20] J. Zhang and Z. Hou, "Experimental study on simulation materials for solid-liquid coupling," *Chinese Journal of Rock Mechanics and Engineering*, vol. 23, pp. 3157–3161, 2004.
[21] K. Wang, S. Li, Q. Zhang et al., "Development and application of new similar materials of surrounding rock for a fluid-solid coupling model test," *Rock and Soil Mechanics*, vol. 37, pp. 2521–2533, 2016.
[22] T. Han, W. Yang, and Z. Yang, "Development of similar material for porous medium solid-liquid coupling," *Rock and Soil Mechanics*, vol. 32, pp. 1411–1417, 2011.
[23] H. Zhou, Y. Tang, and D. Hu, "Study on coupled penetrating-dissolving model and experiment for salt rock cracks," *Chinese Journal of Rock Mechanics and Engineering*, vol. 25, pp. 946–950, 2006.
[24] Z. Li, M. Ma, and Y. Bao, "Development and application of fluid-solid coupling similar materials in discharge test of Old Goaf water," *Geofluids*, vol. 2020, Article ID 8834885, 2020.
[25] Y. Wu, "Study on the relationship between stress and seepage in fractured rock mass," *Hydrogeology & Engineering Geology*, vol. 22, pp. 30–35, 1995.
[26] M. Ren, Q. Zhang, and S. Chen, "Physical model test study on synergistic action of liningrock for deep tunnel under complex geological conditions," *China Civil Engineering Journal*, vol. 52, pp. 98–109, 2019.
[27] Q. Y. Zhang, M. Y. Ren, K. Duan et al., "Geo-mechanical model test on the collaborative bearing effect of rock-support system for deep tunnel in complicated rock strata," *Tunnelling and Underground Space Technology*, vol. 91, Article ID 103001, 2019.